ACS APPLIED MATERIALS & INTERFACES

Research Article

www.acsami.org

Surface-Confined Heterometallic Triads on the Basis of Terpyridyl Complexes and Design of Molecular Logic Gates

Prakash Chandra Mondal,*[,†,‡,⊥] Vikram Singh,[†] Yekkoni Lakshmanan Jeyachandran,[§,#] and Michael Zharnikov*[,§]

[†]Department of Chemistry, University of Delhi, Delhi 110007, India

[‡]Department of Chemical Physics, Weizmann Institute of Science, Rehovot 76100, Israel

[§]Applied Physical Chemistry, Heidelberg University, Heidelberg 69120, Germany

Supporting Information

ABSTRACT: Surface-confined heterometallic molecular triads (SURHMTs) were fabricated on SiO_x-based solid substrates using optically rich and redox-active Fe-, Os-, and Ru-based terpyridyl complexes as metalloligands and Cu^{2+} ions as linkers. Optical and electrochemical studies reveal efficient electronic intramolecular communication in these assemblies. The UV−vis spectra of the triads exhibit a superposition of the metal-to-ligand charge-transfer bands of individual complexes, providing a significant enlargement of the optical window, useful for application. Similarly, cyclic voltammograms of SURHMT layers show a variety of redox peaks corresponding to individual complexes as well as multi-redox states at a low potential. Interaction of a representative SURHMT assembly with redox-active $NOBF_4$ was investigated and used as a basis for configuring molecular logic gates.

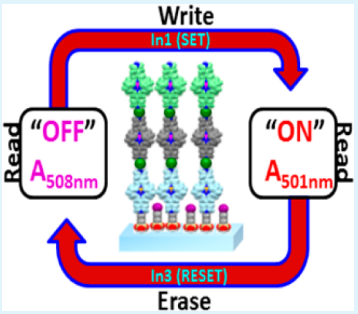

KEYWORDS: *metallo-ligands, layer-by-layer, molecular triads, logic gates, redox states*

INTRODUCTION

Since the advent of coordination chemistry, transition metal complexes have attracted significant interest of both academic and industrial communities, in view of their flexible molecular design, versatile physical and chemical properties, and a variety of potential applications. A particular advantage of these complexes is a possibility to immobilize them on various solid substrates as monolayers, oligomer wires, metallo-organic assemblies, etc.[1−6] Such assembles are a good alternative and a useful addition to the analogous systems based on the coordination of organic ligands by metal ions as well as to increasingly popular metal−organic frameworks.[7−9] These assemblies, which can also be considered as surface-confined inorganic−organic hybrid materials,[10,11] likely offer a potential route to different applications, including sensors, switches, memory elements, logic integration, electrochromic films, and photonic materials,[12−16] to name a few.

Popular systems in this context are transition-metal-based polypyridyl complexes, which became a focal point in diverse research areas due to their tunable photophysical[17,18] and electrochemical properties[19] as well as potential applications in molecular electronics,[20] catalysis,[21] solar energy conversion,[22,23] etc. Most of these applications rely on controlled immobilization of the polypyridyl complexes on solid substrates. Such an immobilization was indeed successively performed in form of monolayers, molecular dyads, as well as homogeneous and heterogeneous oligomer films, with individual polypyridyl complexes serving as molecular building blocks.[24−27] The primary methodology to build the above systems is stepwise coordination reaction of the individual complexes (metalloligands) and inorganic coupling units. This methodology has potential to create even more complex molecular assemblies of novel architectures, with desired thickness, structure, orientation, and physicochemical properties.[28−31]

Along these lines, we report here the fabrication of surface-confined heterometallic molecular triads (SURHMTs) on glass, Si (100), and indium tin oxide (ITO)-coated glass substrates. For this purpose we used well-known terpyridyl complexes[32] (so-called metalloligands), specifically, $Fe(pytpy)_2{\cdot}2PF_6$, $Ru(pytpy)_2{\cdot}2PF_6$, and $Os(pytpy)_2{\cdot}2PF_6$ (pytpy = 4′-(4-pyridyl)-2,2′:6′,2″-terpyridyl) as the molecular building blocks (Scheme 1) and Cu^{2+} ions as the metallolinkers. These metalloligands are abbreviated below as Fe-PT, Ru-PT, and Os-PT, respectively. They were chosen due to their strong binding affinity to the transition metal ions, tunable photophysical and electrochemical properties (based on the well-separated optical bands and redox peaks, respectively), as well as expected electronic communication between individual M-PT units (M = Fe, Ru, Os) within the derived assemblies.[33] This communication is assumed to be mediated by conductive metallolinkers (Cu^{2+}) and is superior to the case of organic linkers, which can be potentially advantageous for molecular electronics applications. To the best of our knowledge, this is the first report on heterogeneous molecular triads, where three different metallo-

Received: February 1, 2015
Accepted: April 8, 2015
Published: April 8, 2015

DOI: 10.1021/acsami.5b00953
ACS Appl. Mater. Interfaces 2015, 7, 8677−8686

Scheme 1. Schematic Representation of the Fabrication Procedure for SURHMTs by the Example of the Fe-PT/Cu/Ru-PT/Cu/Os-PT Assembly[a]

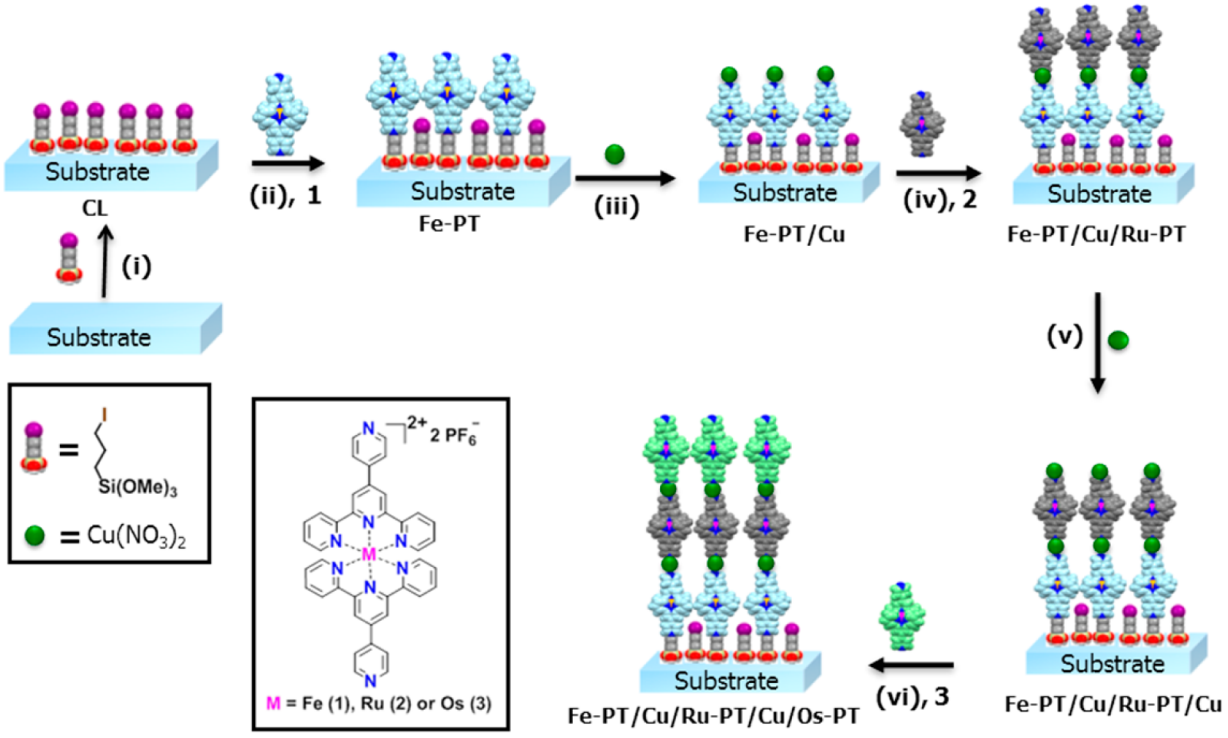

[a](i) Immobilization of 3-iodo-*n*-propyl-trimethoxysilane on a SiO_x substrate to form coupling layer (CL), (ii) quaternization of pendant pyridyl group of M-PT (M = Fe^{2+}, Ru^{2+}, Os^{2+}) to form template layer (TL), (iii) coordination of $Cu(NO_3)_2$ with pyridine-terminated monomolecular template layer to form Cu-terminated template layer, (iv) coordination of a different M-PT unit, (v) coordination of Cu^{2+}, and (vi) coordination of the third M-PT unit to form the desired SURHMT.

ligands of group VIII transition metal ions (Fe^{2+}, Ru^{2+}, and Os^{2+}) were assembled together on a single platform and studied in context of their optical and electrochemical properties. Among other advantages, a combination of three different metallo-organic units in one functional moiety increases the parameter space, allowing to store more "bits of information", which has potential applications in the development of molecular memory.[16,34]

EXPERIMENTAL SECTION

Synthesis and characterization data for the 4′-pyridyl terpyridyl and the derived Fe-PT, Ru-PT, and Os-PT complexes are given in the Supporting Information (Scheme S1 and Figure S1), along with a detailed description of all fabrication steps for the preparation of the triad films.

RESULTS AND DISCUSSION

General Design and Fabrication of Surface-Confined Heterometallic Molecular Triads. The SURHMT assemblies were fabricated by stepwise coordination reactions of metallolinkers and metalloligands with pyridine-terminated template layers (Scheme 1; see the Supporting Information for details) following the established strategy of our previous publications.[24−27] Initially, an iodine-terminated coupling layer (CL) was formed, serving as substrate for the attachment of the first M-PT unit (M = Fe^{2+}, Ru^{2+}, Os^{2+}). The resulting monomolecular template layer was allowed to react with $Cu(NO_3)_2$ in acetonitrile. Subsequently, the Cu-terminated template layer was immersed in a solution containing a dissimilar M-PT unit to fabricate a heterometallic molecular dyad. Finally, reaction with $Cu(NO_3)_2$ and subsequent coordination with a dissimilar M-PT unit were repeated once more, resulting in a SURHMT. Combining different M-PT units, different SURHMTs were fabricated.

Basic Characterization of the Intermediate Layers and Molecular Triads. Formation of SURHMTs was monitored by static water contact angle (CA) goniometry, atomic force microscopy (AFM), spectroscopic ellipsometry, X-ray photoelectron spectroscopy (XPS), and near-edge X-ray absorption fine structure (NEXAFS) spectroscopy. Representative of all possible combinations of the M-PT units within a triad, Fe-PT/Cu/Ru-PT/Cu/Os-PT assembly was chosen, but also some selected data for other triads are presented.

Contact Angle. The CA goniometry measurements on the representative Fe-PT template layer showed a moderately hydrophobic surface, associated with a free pyridine group, with a CA of 76 ± 2° (Supporting Information, Figure S2a). In contrast, Cu-terminated Fe-PT template layer (Fe-PT/Cu) had a lower value of CA, namely, 58 ± 0.5° (Supporting Information, Figure S2b), which agrees with the expected hydrophilicity of the Cu^{2+} ions. For the final triad assemblies, a CA of 74−83° was observed, similar to the Fe-PT template layer, which is understandable in view of the same termination by the pyridine moieties.

Atomic Force Microscopy. A tapping mode AFM image of the representative Fe-PT template layer on Si showed a relatively smooth film (see Figure S3a in the Supporting Information). The root-mean-square roughness (R_{rms}) measured for this layer over a scan area of 500 × 500 nm^2 was estimated at 0.56 ± 0.03 nm. Such a low roughness value

DOI: 10.1021/acsami.5b00953
ACS Appl. Mater. Interfaces 2015, 7, 8677−8686

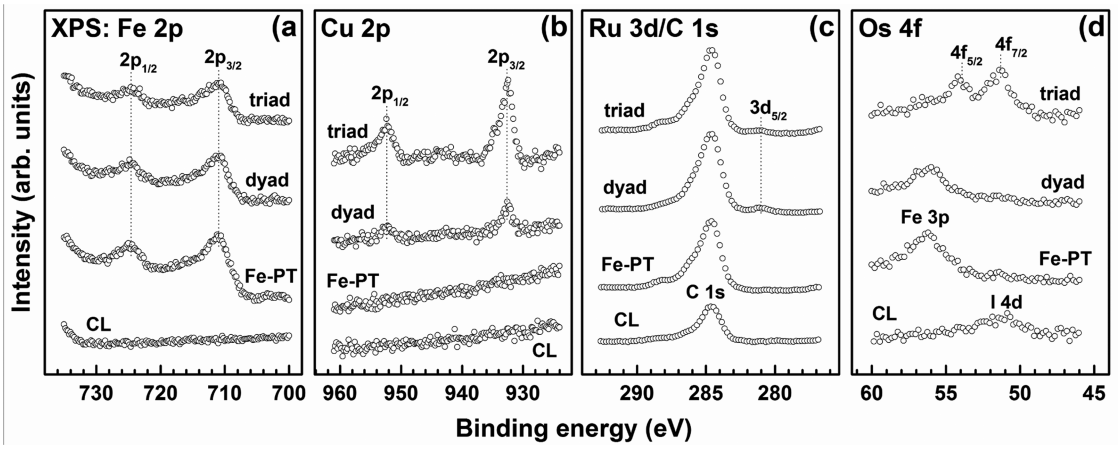

Figure 1. Fe 2p (a), Cu 2p (b), C 1s/Ru 3d (c), and Os 4f (d) XP spectra of the coupling (CL), template (Fe-PT), dyad (Fe-PT/Cu/Ru-PT), and triad layers for the Fe-PT/Cu/Ru-PT/Cu/Os-PT assembly on Si(100). The characteristic emissions are marked. All assignments are performed in accordance with ref 35.

suggests the formation of a uniform film without contamination or physisorbed molecules. The R_{rms} value increased to 0.78 ± 0.08 nm and further to 0.99 ± 0.1 nm for the dyad (Fe-PT/Cu/Ru-PT) and triad (Fe-PT/Cu/Ru-PT/Cu/Os-PT) layers, respectively, suggesting a progressive increase of roughness in the course of the successive coordination. The corresponding AFM images are presented in the Supporting Information (Figure S3b,c, respectively). In addition, variation of roughness as a function of the deposition steps is given in the Supporting Information (Figure S4).

Ellipsometry. For the representative Fe-PT/Cu/Ru-PT/Cu/Os-PT assembly, ellipsometry-derived thicknesses of the Fe-PT template layer and the successive dyad and triad films were found to be ∼18.5, 25−32, and 38−42 Å. The observed gradual increase in the thickness suggested an efficient attachment of the individual building blocks. Comparison of the thickness values with the theoretically optimized length of the M-PT units implies that they are considerably tilted (30−40°) with respect to the surface normal. Note that the individual pyridine rings comprising the terpyridine moieties of a M-PT unit are not coplanar but twisted with respect to one another.

X-ray Photoelectron Spectroscopy. Selected XP spectra, following the successive fabrication of the representative Fe-PT/Cu/Ru-PT/Cu/Os-PT triad layer, are presented in Figure 1; additional XPS data for Si 2p binding energy (BE) region can be found in the Supporting Information (Figure S5). For CL, a weak C 1s emission at a BE of ∼284.6 eV and I 4d doublet at a BE of 51 eV (I $4d_{5/2}$) are observed, in agreement with the expectations. For the Fe-PT template layer, characteristic Fe 2p doublet at BEs of ∼711 eV (Fe $2p_{3/2}$) and 724.8 eV (Fe $2p_{1/2}$) as well as Fe 3p doublet at a BE of ∼56 eV (Fe $3p_{3/2}$) are perceptible, evidencing the coordination of Fe-PT to CL (Figure 1a). For the dyad assembly, additional signals of Cu (Cu $2p_{3/2}$ and Cu $2p_{1/2}$ at BEs of 932.4 and 952.2 eV, respectively, Figure 1b) and Ru (Ru $3d_{5/2}$ at a BE of ∼281.0 eV, Figure 1c) can be traced, manifesting the coordination of Ru-PT to the Cu^{2+} linker. Accordingly, the C 1s intensity increases, and the Fe-related signals get attenuated to some extent as compared to the Fe-PT spectra. Finally, for the triad assembly, a characteristic signal of Os is exhibited (Os $4f_{7/2}$ and Os $4f_{5/2}$ at BEs of 51.4 and 54.2 eV, respectively), indicating the coordination of Os-PT (Figure 1d). Simultaneously, there is a further progressive increase of the C 1s signal and a decrease of the Fe-related signals as well as an increase of the Cu signal (second Cu^{2+} linker) and decrease of the Ru $3d_{5/2}$ signal. In general, the XP spectra in Figure 1 suggest successive coordination of the Fe-PT, Ru-PT, and Os-PT units over the Cu^{2+} linkers, in accordance with the expected architecture of the Fe-PT/Cu/Ru-PT/Cu/Os-PT assembly.

Near-Edge X-Ray Absorption Fine Structure Spectroscopy. The formation of the molecular triads on the SiO_x substrates was additionally monitored by NEXAFS spectroscopy. The respective spectra of the Fe-PT/Cu/Ru-PT/Cu/Os-PT triad, acquired at the C and N K-edges, are presented in Figure 2a,b,

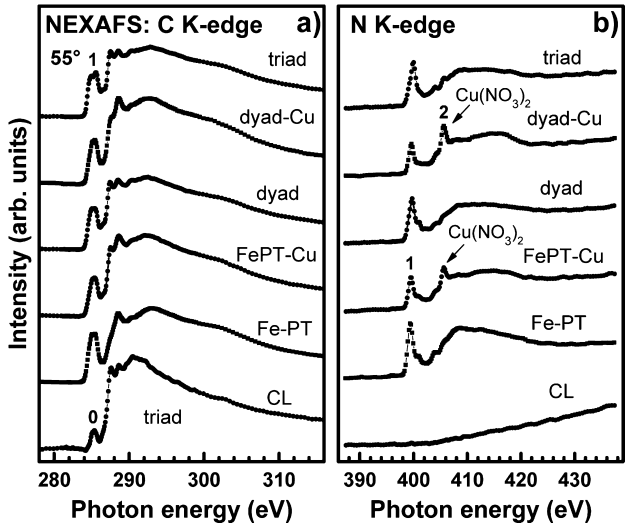

Figure 2. C (a) and N (b) K-edge NEXAFS spectra of the coupling (CL), template (Fe-PT), template-Cu, dyad, dyad-Cu, and triad layers for the Fe-PT/Cu/Ru-PT/Cu/Os-PT assembly on Si(100). The spectra were acquired at an X-ray incidence angle of 55° (magic angle). Some of the characteristic resonances are marked.

respectively. These spectra were collected at so-called magic angle of X-ray incidence (55°), to avoid any effects related to molecular orientation.[36] The C K-edge spectrum of CL exhibits a weak, pre-edge π^* resonance at ∼285.2 eV (**0**), along with a comparable strong absorption edge and several low intense, π^*-like resonances at higher photon energies. The N K-edge spectrum of CL shows no nitrogen signal as can be expected

DOI: 10.1021/acsami.5b00953
ACS Appl. Mater. Interfaces 2015, 7, 8677−8686

from the molecular composition (Scheme 1). In contrast, the analogous spectra of all subsequent layers exhibit a strong π^* resonance at 399.6−399.8 eV (**1**), characteristic of the pyridine[37] and terpyridine[38,39] moieties in the Fe-PT, dyad, and triad assemblies. Interestingly, this resonance is accompanied by another one, at ∼405.7 eV (**2**), in the case of the Cu-terminated layers. We believe that the latter feature corresponds to the residuals of the NO_3 groups still attached to the terminal Cu^{2+} ions.[40] The characteristic absorption structure of pyridine[37] and terpyridine moieties[38] is also observed in the C K-edge spectra, for all successive layers, coordinated to CL. The major feature is a double, pre-edge π^*-like resonance at ∼284.9 and ∼285.7 eV (**1**), with these values varying slightly through the series. Such a double peak is related to the different C 1s core binding energies of the carbon atoms in the different positions within the pyridine ring.[41] Along with the magic-angle NEXAFS spectra, those at X-ray incidence angles of 20° and 90° were acquired to look for so-called linear dichroism effects, namely, the dependence of the absorption resonance intensity on the incidence angle of the linearly polarized light.[36] Such a dependence is usually observed for highly oriented molecular ensembles as far as the characteristic, average tilt angle of involved molecular orbitals differs noticeably from the magic angle of 54.7°.[36] In the given case, for all layers within the Fe-PT/Cu/Ru-PT/Cu/Os-PT assembly, no linear dichroism was observed (Supporting Information, Figures S6 and S7). On one hand, this can mean a lack of the orientational order, but, on the other hand, it may correspond to an average tilt angle of ∼35° for the pyridine rings (corresponding to ∼54.7° for the respective π^* orbitals). The latter explanation seems to be more realistic, in view of the ellipsometry data (see above).

Optical Properties. UV−vis spectra of several representative triads as well as the spectra of the corresponding template (monolayer) and dyad layers are presented in Figure 3, along with the "baseline" spectrum of the glass substrate. The spectra of the Fe-PT, Ru-PT, and Os-PT monolayers, serving as the references for the individual building blocks of the triads, are given in Figure 3a,c,d, respectively. These spectra exhibit characteristic metal-to-ligand charge-transfer (MLCT; dπ(M = Fe, Ru, Os)-π^*(4′-pytpy) process) bands at 586 nm (Fe-PT) and 505 nm (Ru-PT) as well as at 505 and 694 nm (Os-PT). For all four M-PT combinations presented in Figure 3, the spectra of the individual building blocks superimpose on one another, first upon the assembly of the dyads, and then upon the formation of the triads. The relative intensities of the M-PT-related MLCTs bands differ somehow for different arrangements, but all these bands are clearly present in the overall spectra of the triads, covering the entire spectral range from 400 to 800 nm. The presence of such bands, associated with the specific M-PT units, gives broad possibilities for the design of versatile sensors and related logic gates as will be discussed below. The analysis of the UV−vis data for a representative Fe-PT/Cu/Ru-PT/Cu/Os-PT assembly gives information about the surface coverage and the efficiency of coordination in the triad layers. The surface coverage of the Fe-PT template layer on glass, Γ, was estimated at 6.6×10^{13} metalloligands/cm^2 (i.e., ∼1.51 nm^2/metalloligand), in good agreement with our previous reports;[26,27,42] this value was calculated using the equation $\Gamma = (N_A A_\lambda)/2\varepsilon_\lambda$, where N_A is the Avogadro's constant and A_λ and ε_λ are, respectively, the absorbance and the isotropic molar extinction coefficient at wavelength λ. Note that the surface coverage observed was below an ultimate limit of $\sim 1 \times 10^{14}$ metalloligands/cm^2 (i.e., ∼1 nm^2/metalloligand) given by the cross section of the M-PT moieties, so that the interaction between individual triads was limited, and an even closer packing was, in principle, possible. The surface coverage of the dyad and triad layers was estimated at 6.01×10^{13} metalloligands/cm^2 (1.66 nm^2/metalloligands) and 5.3×10^{13} metalloligands/cm^2 (1.88 nm^2/metalloligands), respectively. These values give the yield of the dyad and triad assemblies of ∼91% and ∼80%, respectively, with respect to the monolayer template. Analogous values were observed for other triads, suggesting a rather high efficiency of the coordination reactions involved.

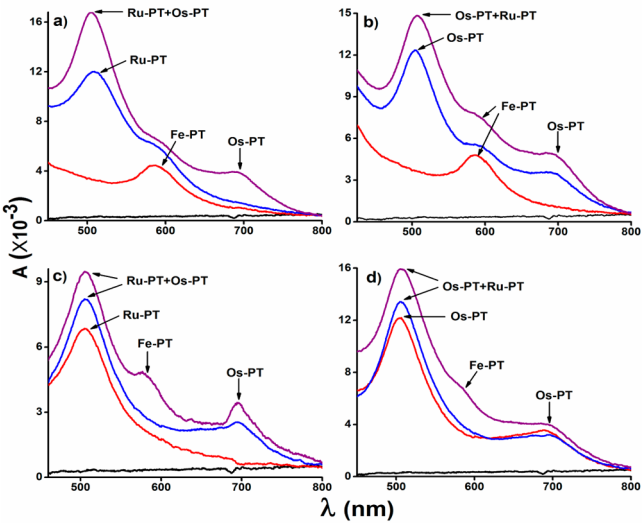

Figure 3. UV−vis spectra of Fe-PT/Cu/Ru-PT/Cu/Os-PT (a), Fe-PT/Cu/Os-PT/Cu/Ru-PT (b), Ru-PT/Cu/Os-PT/Cu/Fe-PT (c), and Os-PT/Cu/Ru-PT/Cu/Fe-PT (d) layers on glass substrates. Black, red, blue, and purple solid lines represent the spectra of the glass substrate ("baseline") and the template, dyad, and triad layers, respectively. The characteristic MLTC bands are marked.

Additional information can be obtained by a detailed analysis of the UV−vis spectra. An important observation is red shifts of the MLCT bands associated with the individual building blocks (M-PT) as compared to the solution (acetonitrile) spectra (see Figure S8 in the Supporting Information). These shifts are most likely related to quaternization of the pyridine group and/or cofacial orientation of the molecules within the purview of exciton theory.[25,43,44] They amount to 17−19 nm in the case of the representative Fe-PT/Cu/Ru-PT/Cu/Os-PT film and are accompanied by additional shifts of the MLCT bands in the course of the coordination steps (Figures 3a). In particular, for the Fe-PT/Cu/Os-PT/Cu/Ru-PT assembly (Figure 3b), the position of the Fe-PT MLCT band changed from 586 nm for the template layer to 597 and 590 nm for the dyad and triad layers, respectively. This phenomenon is especially important since it suggests an efficient intramolecular electronic communication between the individual M-PT units within the triads. Since Ru-PT is kinetically more inert and has a larger highest occupied molecular orbital−lowest unoccupied molecular orbital gap, it tends to withdraw the electron density from Fe-PT and Os-PT, which should lead to a blue shift of the MLCT band, exactly as observed in the UV−vis spectra in Figure 3.

Further important parameters of the metallo-organic assemblies are full width at half-maximum (FWHM) of the

DOI: 10.1021/acsami.5b00953
ACS Appl. Mater. Interfaces 2015, 7, 8677−8686

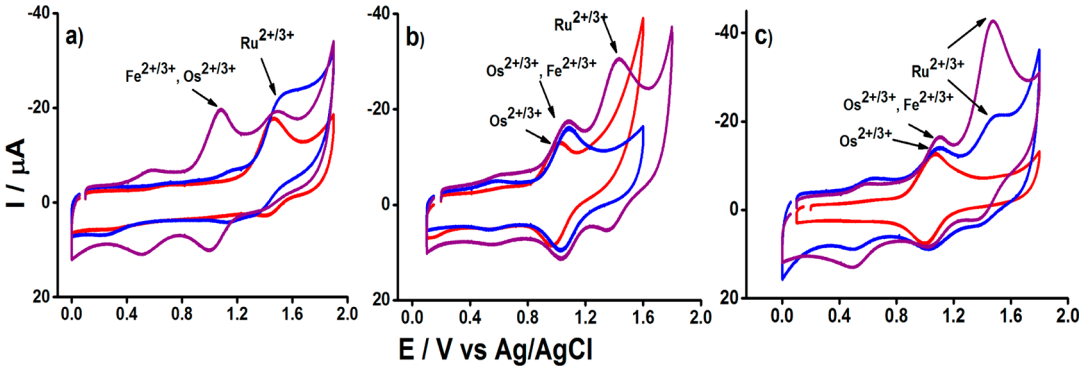

Figure 4. CVs of Ru-PT, Ru-PT/Cu/Fe-PT, and Ru-PT/Cu/Fe-PT/Cu/Os-PT layers (a), Os-PT, Os-PT/Cu/Fe-PT, and Os-PT/Cu/Fe-PT/Cu/Ru-PT layers (b), and Os-PT, Os-PT/Cu/Ru-PT, and Os-PT/Cu/Ru-PT/Cu/Fe-PT layers (c) on ITO-coated glass substrates. Red, blue, and purple solid lines represent the cyclic voltammograms of the corresponding template, dyad, and triad layers, respectively. The cyclic voltammograms were recorded at 200 mV s^{-1}. The characteristic redox processes ($M^{2+/3+}$, where M = Fe, Ru, and Os) are marked.

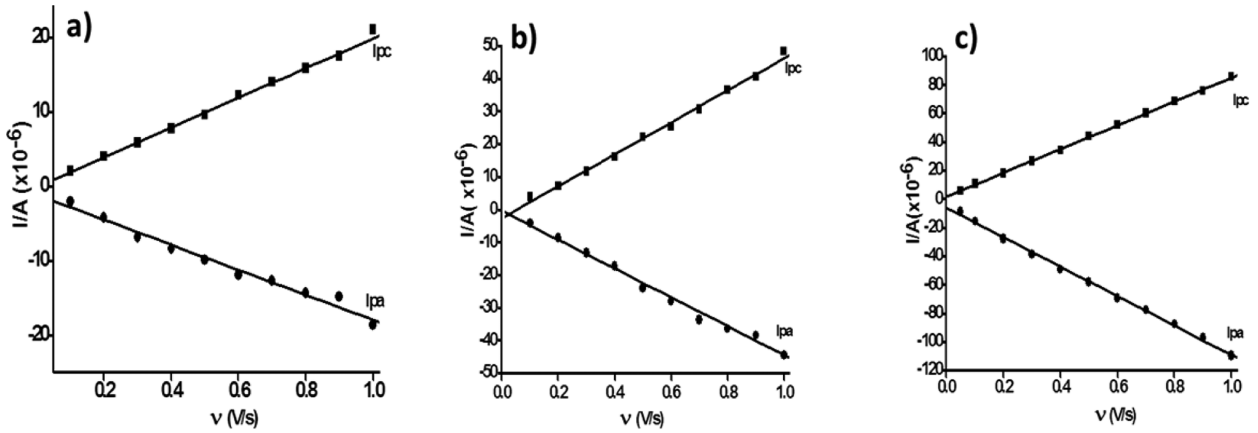

Figure 5. Linear behavior (R^2 = 0.98−0.99) of the peak current densities (cathodic and anodic currents) as functions of the scan rates (ν) for the Fe-PT (a), Ru-PT (b), and Os-PT (c) template layers on ITO-coated glass substrates.

MLCT bands and optical band gap (E_g). For the Fe-PT/Cu/Ru-PT/Cu/Os-PT case, FWHM of the MLCT band of the Fe-PT template layer was estimated at ∼58 nm, which is larger by ∼7 nm than the analogous value in acetonitrile solution. A similar band broadening was observed for the Ru-PT and Os-PT moieties. This effect can be tentatively explained by intermolecular interactions in the densely packed films.[44] Note that FWHM of the MLCT band increased even further in the dyad and triad layers, which can be considered as a further evidence of the intramolecular communication between the individual M-PT units within the triads.

Optical band gap (E_g) for the template (Fe-PT), dyad, and triad layers on glass substrate was evaluated by extrapolating the MLCT band and estimated at 1.84, 1.79, and 1.61 eV, respectively, which is substantially lower than the values obtained in acetonitrile.[26] A progressive narrowing of the optical band gap shows a potential of multi-M-PT assemblies for design of metallo-organic materials.

Electrochemical Properties. Electrochemical properties of the template, dyad, and triad layers on ITO-coated glass substrates were investigated using cyclic voltammetry (CV, Figure 4). The active surface area of the electrodes was kept at ∼2.1 cm^2. The template layers showed single-electron oxidation and reduction processes at +1.18/1.14 (Fe-PT), +1.46/1.42 (Ru-PT), and +1.03/0.99 V (Os-PT) (vs Ag/AgCl), respectively (see Figure S9 in the Supporting Information for the solution data). Accordingly, the half-wave redox potentials $E_{1/2}$ for the Fe-PT, Ru-PT, and Os-PT template layers were estimated at +1.16, +1.44, and +1.01 V, respectively. A linear behavior (R^2 = 0.98−0.99) of the peak current densities (cathodic and anodic currents) as functions of the scan rate shown in Figure 5 unequivocally suggests that the electrochemical process in the M-PT template layers is diffusionless. In addition, the template layers showed excellent thermal stability (up to 200 °C) and high redox stability (>1 × 10^3 "read"−"write" cycles; see Figures S10 and S11 in the Supporting Information).

Significantly, there are shifts of the redox potentials upon the triad assembly, which can be clearly seen by the example of the Ru-PT/Cu/Fe-PT/Cu/Os-PT heterotriad. For the respective Ru-PT/Cu/Fe-PT dyad layer, an oxidation peak at +1.53 V assigned to the $Ru^{2+/3+}$ center was anodic shifted by ∼70 mV as compared to that in the template layer (Figure 4a). Upon the successive assembly of Os-PT (triad), the oxidation potential decreases further to +1.48 V. At the same time, a merging of oxidation and reduction peaks associated with the $Fe/Os^{2+/3+}$ redox processes was observed at +1.08/1.0 V, exhibiting a cathodic shift of 100 mV in the triad layer (Ru-PT/Cu/Fe-PT/Cu/Os-PT) as compared to the dyad layer (Ru-PT/Cu/Fe-PT) (Figure 4a). These observations indicate the presence of electronic communication between the metalloligands in the triad assembly. Significantly, a similar conclusion was derived on the basis of the UV−vis spectra where the MLCT band of the Fe-PT showed a blue shift of 7 nm upon the coordination

DOI: 10.1021/acsami.5b00953
ACS Appl. Mater. Interfaces 2015, 7, 8677−8686

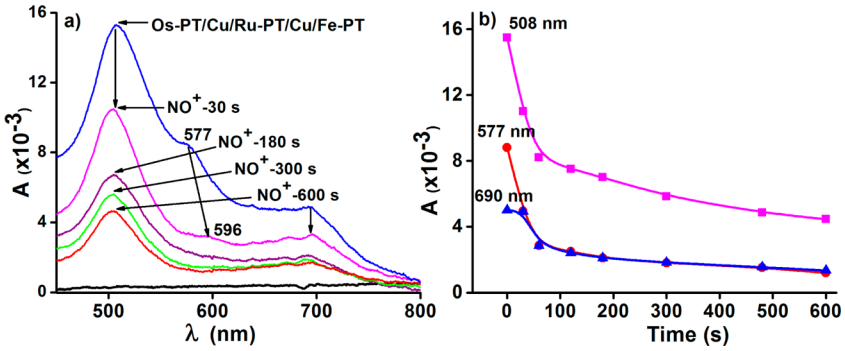

Figure 6. (a) Ex situ UV−vis spectra of Os-PT/Cu/Ru-PT/Cu/Fe-PT triad layer before and after exposure to 100 ppm of $NOBF_4$ (release of NO^+) in dry acetonitrile for a certain time (marked at the curves) and (b) absorbance of the most prominent MLCT bands (λ_{max} at 508, 577, and 690 nm) as a function of the exposure time.

of Ru-PT to the Fe-PT/Cu/Os-PT dyad. Further, relatively low values (~35−50 mV) in the peak-to-peak separation ΔE_p, between the anodic and cathodic processes, reveal a confinement of the metalloligands on the conductive substrates.

Similar observations were made with the other heterotriads. For example, the Os-PT/Cu/Fe-PT/Cu/Ru-PT layer exhibited single-electron redox process at +1.43 V ($Ru^{2+/3+}$) and a merging of oxidation/reduction features for $Fe/Os^{2+/3+}$ at +1.08 and +1.04 V as shown in Figure 4b. The oxidation feature was anodic shifted by 70 mV as compared to the Os-PT template. The $E_{1/2}$ value for the Ru-center in the heterotriad was estimated at +1.38 V, which corresponds to a noticeable cathodic shift (by ~60 mV) as compared to the Ru-PT layer (vide supra). The decrease in the $E_{1/2}$ value is an indication for the transfer of electron density from the Fe-PT and Os-PT units toward the Ru-center of the Ru-PT moiety in the triad assembly. Also the Os-PT/Cu/Ru-PT/Cu/Fe-PT heterotriad showed similar trend in its redox behavior (Figure 4c). In particular, FWHM values of the oxidation peak, $\Delta E_{pa,1/2}$, in the template, dyad, and triad layers were estimated in the range of +120−210 mV, which deviate from an ideal Nernstian electrochemical relation ($\Delta E_{P,1/2}$ = 90/n mV).[45] This anomaly could be related to the interaction between the redox sites and/or their heterogeneity.[42,46,47] In addition to the redox peaks discussed above, there are also some features at lower potentials (+0.5 to +0.6 V) that are most likely related to the formation of a mixed-valence redox species.[26] Interestingly, these features are not prominent for the dyad layers but well-perceptible for the triad assemblies.

Significantly, the distinct redox states (oxd/red) in the heterometallic triads can be considered as equivalent to the change of a bit of information (either "0" or "1"). Considering both M-PT related and the mixed-valence redox processes, four well-defined redox states can be achieved which are 000, 100, 110 (two-oxidized) and 111. The 000 memory setting is associated with the nonoxidized state at a relatively lower potential (less than 0.3 V); the 100 setting indicates one oxidation state at +0.5 to +0.6 V; 110 corresponds to two oxidation states at 1.2 V; and 111 is akin to three oxidized states at relatively high potential (more than 1.42 V). Interestingly, the oxidized redox states can be reconfigured in the original states (M^{2+}) by applying the corresponding reduction potential. The charge retention time of individual systems can be modified by introducing a barrier between the metalloligand and the conductive substrates.[48]

Note that after recording the voltammograms, the electrolyte solution was cross-checked by UV−vis and CV measurements, but no optical or redox signal related to the released metalloligands was observed. These experiments clearly indicate that there was no desorption of the M-PT units during the CV experiments. In addition, the triad systems showed good electrochemical stability under electrochemical stress of +2 V, underlining a high quality of these assemblies.

Interaction of Molecular Triad with NO⁺. The heterometallic molecular triads were utilized for detection of small, redox-active molecules. For instance, the redox-active $NOBF_4$ induced selective oxidation of the metal centers (Fe/Os) in the Os-PT/Cu/Ru-PT/Cu/Fe-PT layers on glass substrate, which could be monitored by UV−vis spectroscopy in the visible range. The triad film was exposed to a dry acetonitrile solution containing 100 ppm of $NOBF_4$. Subsequently, changes in the UV−vis spectra were monitored as a function of time (Figure 6), tracing the effect of the NO^+ ions forming upon the dissolving of $NOBF_4$. When the triad layer was immersed in the $NOBF_4$ solution for 30 s, the MLCT band at λ_{max} = 577 nm associated with the Fe-PT unit exhibited a bathochromic shift by 19 nm, along with a simultaneous decrease in absorbance (by ~60%) as depicted in Figure 6a. These changes were attributed to quaternization of the free pyridyl group by NO^+ followed by oxidation of Fe^{2+} to Fe^{3+}.[43] Additionally, the joint ^{1}MLCT transition at λ_{max} = 508 nm was blue-shifted by 7 nm, accompanied by a significant decrease in absorbance. Full oxidation of the metal centers, M^{2+} to M^{3+} (M = Fe, Os) was observed within 10 min as corroborated by diminishing MLCT bands of Fe-PT and Os-PT (Figure 6). Interestingly, the Fe-center got oxidized faster than the Os-center, even though the former one has a higher oxidation potential than that of the latter one. This observation can be tentatively explained by the fact that the Fe center experienced a stronger effect of NO^+ than the Os center, since the Fe-PT moiety constitutes the topmost part of the triad layer. Notably, the Ru-center in the triad layer did not get oxidized, as confirmed by the presence of the MLCT band at 501 nm even after the $NOBF_4$ exposure for 10 min. This can be expected since the oxidation potential of the Ru center is higher than that of the Fe/Os centers (vide supra). Probably, there is a transfer of electron density from the Fe/Os centers toward the Ru center in the triad assembly. Note that the time required for the oxidation was found somewhat shorter than that for the individual M-PT (M = Fe, Os) template layer(s). Importantly, the original spectrum was recovered after the addition of H_2O and Et_3N to the solution, as the former one reduces the metal centers (Fe/Os^{3+}), while the latter one dequaternizes NO^+ from the pyridyl group (see

DOI: 10.1021/acsami.5b00953
ACS Appl. Mater. Interfaces 2015, 7, 8677−8686

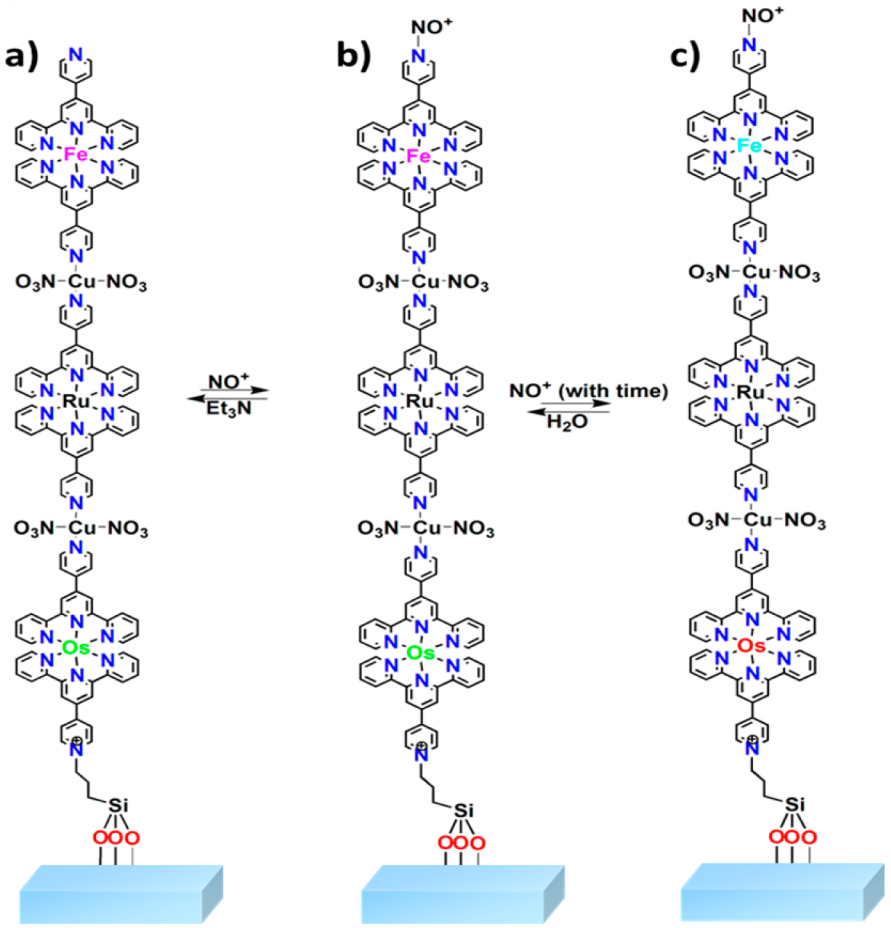

Figure 7. Most plausible mechanism of oxidation/reduction and quaternization/dequaternization of Os-PT/Cu/Ru-PT/Cu/Fe-PT on glass substrates; neutral form of triad (a), quaternized form of triad upon reaction with NO^+ (b), and quaternized−oxidized form of the metal centers (Os^{3+}, Fe^{3+}) in the triad (c). The reversibility can be achieved using H_2O and Et_3N as shown in Figure 12 in the Supporting Information.

Supporting Information, Figure S12). On the basis of the above experimental results, a plausible mechanism of the relevant processes was proposed, as shown in Figure 7. Note that this mechanism is additionally supported by the experiments with the Fe-PT solution (in acetonitrile) as described in our previous report.[43]

Development of Molecular Logic Gates. In general, molecular assemblies that are capable of performing physicochemical changes as reaction to external stimulus can serve as switches or Boolean logic at the molecular level.[13,49−54] A particular useful building block for information processing and computing devices at the nanoscale is a molecular logic gate. Such a gate can be constructed on the basis of the heterotriads such as Os-PT/Cu/Ru-PT/Cu/Fe-PT. As shown in previous section, exposure of the triad layer to $NOBF_4$ resulted in the oxidation of the Os^{2+} centers in the assembly, accompanied by diminishing the ^{3}MLCT band at 690 nm and blue shift of the ^{1}MLCT band from 508 to 501 nm. Upon addition of NO^+, the MLCT band at 577 nm shows a red shift before the Fe^{2+} centers gets oxidized. The initial spectrum can, however, be restored by addition of 5 μL of deionized H_2O, corresponding to the water-induced reduction of Fe^{3+}/Os^{3+} to Fe^{2+}/Os^{2+} state, which is a well-established phenomenon.[43,55] The respective reversible changes of the optical properties can be used to build logic gates at the molecular scale. To develop such devices, the chemical inputs (NO^+, H_2O, Et_3N) and optical outputs (absorbance at 577 nm and MLCT at 501 nm) were coded with Boolean logic functions, which are 0 for the OFF state and 1 for the ON state.[49] Chemical information processing with NO^+, H_2O, and Et_3N inputs were considered as Input1, Input2, and Input3, respectively, while absorbance at 577 nm was considered as Output1. The present system configures a combinatorial logic gate (Figure 8).

While monitoring the oxidation of Os^{2+} center in the assembly, time is considered as one of the inputs, since the metal center gets oxidize slowly upon NO^+ stimuli. Assuming

In1 (NO^+)	In2 (H_2O)	In3 (Et_3N)	Out1 ($A_{577\ nm}$)
0	0	0	1
0	0	1	1
0	1	0	1
0	1	1	1
1	0	0	0
1	0	1	1
1	1	0	1
1	1	1	1

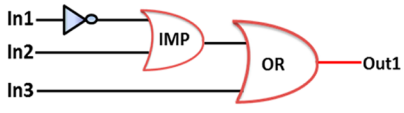

Figure 8. Truth table (left) and schematic (right) for a Boolean logic gate on the basis of the Os-PT/Cu/Ru-PT/Cu/Fe-PT heterotriads. The gate has NO^+, H_2O, and Et_3N as inputs, namely, In1, In2, and In3, respectively, while absorbance at 577 nm serves as output (out1).

DOI: 10.1021/acsami.5b00953
ACS Appl. Mater. Interfaces 2015, 7, 8677−8686

NO^+, time (min), H_2O, and Et_3N as In1, In2, In3, and In4, respectively, while monitoring the MLCT band at 501 nm as output2 (Out2), the present chemical process allows us to design an even more complex logic gate at the molecular scale. The truth table and four input-based logic circuit diagram (a combination of AND−NOR−AND gates) for this gate are presented in Figure 9. Remarkably, the output $A_{501\ nm}$ can be

In1 (NO^+)	In2 (Time)	In3 (H_2O)	In4 (Et_3N)	Out2 (λ_{501} nm)
0	0	0	0	0
0	0	0	1	0
0	0	1	0	0
0	0	1	1	0
0	1	0	0	0
0	1	0	1	0
0	1	1	0	0
0	1	1	1	0
1	0	0	0	0
1	0	0	1	0
1	0	1	0	0
1	0	1	1	0
1	1	0	0	1
1	1	0	1	0
1	1	1	0	0
1	1	1	1	0

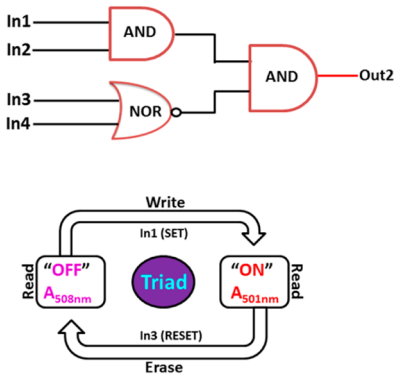

Figure 9. (left) Truth table for the heterotriad based logic gate with all possible variations according to 2^n rule, where n = 4. (right, upper) Combinatorial logic circuits constructed using NO^+, time (min), H_2O, and Et_3N as In1, In2, In3, and In4, while MLCT band at 501 nm as output2 (Out2), respectively. (right, lower) Feedback loop representing a write−read−erase−read cycle upon chemical input on triad assembly.

readily RESET to $A_{508\ nm}$ using an input (In3), while it can be further SET using In1. Thus, the reversible switching behavior (SET/RESET) can be implemented as feedback loop[56] demonstrating a write−read−erase−read cycle (right panel). Chemically driven four-input combinatorial logic gate using a solid support is rare.

An important point is that we used only two of the three available metal centers to design the logic gates described above, based on their specific reaction to the chemical inputs. Potentially, even more complex logic elements can be developed as far as all metal centers of a heterotriad assembly will be utilized. The chemical inputs can be provided by a microfluidic system, allowing a miniaturization of the entire device.

CONCLUSIONS

Using Fe, Ru, and Os terpyridyl complexes as metalloligands and the Cu^{2+} ions as the metallolinkers, surface-confined heterometallic molecular triads were fabricated on glass, Si (100), and ITO-coated glass substrates by stepwise coordination reactions. Formation of SURHMTs was monitored and confirmed by CA goniometry, AFM, spectroscopic ellipsometry, XPS, and NEXAFS spectroscopy. Optical and electrochemical properties of the SURHMT layers were studied in detail and compared to the behavior of the respective template and dyad layers. These studies reveal efficient electronic intramolecular communication in the SURHMT assemblies. The UV−vis spectra of the triads exhibit a superposition of the MLCT bands of individual complexes, providing a significant extension of the optical window to entire visible region (400−800 nm). Similarly, CVs of SURHMT layers show a superposition of redox peaks corresponding to individual complexes as well as distinct multiredox states at a low potential.

The presence of dedicated MLCT bands and redox states associated with the individual metal centers provides a basis for different applications, including sensor fabrication, molecular memory, and molecular logic. Along these lines, significant changes in the optical spectrum of a representative SURHMT layer upon the exposure to external chemical stimuli were demonstrated, complemented by the restoration of the original spectrum upon the effect of another stimulus. This behavior is not only useful for an optical sensor but can also serve as a basis for the design of complex molecular logic gates, as was discussed by the representative examples.

Generally, supported heterometallic molecular assemblies represent a versatile bottom-up strategy allowing design and fabrication of application-specific systems for frontier areas of nanotechnology. The SURHMT layers of the given study are only a representative example in this context. Different combinations of metalloligands and metallolinkers are possible, depending on the requirements of a specific application.

ASSOCIATED CONTENT

Supporting Information

Synthetic detail and characterization data of the 4′-pyridyl terpyridyl and the Fe-PT, Ru-PT, and Os-PT complexes; the design and fabrication of SURHMTs; additional XPS and NEXAFS data; UV−vis and CV solution data for the Fe-PT, Ru-PT, and Os-PT complexes; ^{1}H NMR spectra; discussion of activation of substrates, formation of coupling and template layers, fabrication of heteromolecular triads, materials and methods, thermal and electrochemical stability of template layers; illustration of water contact angles; AFM topography images; plot of roughness versus deposition; reversibility test. This material is available free of charge via the Internet at http://pubs.acs.org.

AUTHOR INFORMATION

Corresponding Authors

*E-mail: mondalpc@gmail.com. Phone: +972 54 797 8617. (P.C.M)

*E-mail: Michael.Zharnikov@urz.uni-heidelberg.de. Phone: +49 6221 544921. (M.Z)

Present Addresses

[⊥]Department of Chemical Physics, Weizmann Institute of Science, Rehovot 76100, Israel.

[#]Department of Physics, Bharathiar University, Coimbatore 641046, India.

Notes

The authors declare no competing financial interest.

ACKNOWLEDGMENTS

This research was financially supported by the Dept. of Science and Technology (SR/NM/NS-12/2010), Univ. of Delhi, New Delhi, India, and the German Research Society (ZH 63/14-2). P.C.M thanks CSIR, New Delhi, for senior research fellowship.

DEDICATION

A tribute to late Prof. T. Gupta, Dept. of Chemistry, Univ. of Delhi, New Delhi, India.

DOI: 10.1021/acsami.5b00953
ACS Appl. Mater. Interfaces 2015, 7, 8677−8686

REFERENCES

(1) Altman, M.; Zenkina, O.; Evmenenko, G.; Dutta, P.; van der Boom, M. E. Molecular Assembly of a 3D-Ordered Multilayer. *J. Am. Chem. Soc.* **2008**, *130*, 5040−5041.

(2) Terada, K.; Nakamura, H.; Kanaizuka, K.; Haga, M.; Asai, Y.; Ishida, T. Long-Range Electron Transport of Ruthenium-Centered Multilayer Films via a Stepping-Stone Mechanism. *ACS Nano* **2012**, *6*, 1988−1999.

(3) Maeda, H.; Sakamoto, R.; Nishihara, H. Metal Complex Oligomer and Polymer Wires on Electrodes: Tactical Construction-sand Versatile Functionalities. *Polymer* **2013**, *54*, 4383−4403.

(4) Nishihara, H.; Kanaizuka, K.; Nishimori, Y.; Yamanoi, Y. Construction of Redox- and Photo-functional Molecular Systems on Electrode Surface for Application to Molecular Devices. *Coord. Chem. Rev.* **2007**, *251*, 2674−2687.

(5) Kurita, T.; Nishimori, Y.; Toshimitsu, F.; Muratsugu, S.; Kume, S.; Nishihara, H. Surface Junction Effects on the Electron Conduction of Molecular Wires. *J. Am. Chem. Soc.* **2010**, *132*, 4524−4525.

(6) M. Haga, M.; Takasugi, T.; Tomie, A.; Ishizuya, M.; Yamada, T.; Hossain, M. D.; Inoue, M. Molecular Design of a Proton-induced Molecular Switch based on Rod-shaped Ru Dinuclear Complexes with bis-tridentate 2,6-bis(benzimidazol-2-yl)pyridine Derivatives. *Dalton Trans.* **2003**, 2069−2079.

(7) Shekhah, O.; Wang, H.; Paradinas, M.; Ocal, C.; Schüpbach, B.; Terfort, A.; Zacher, D.; Fischer, R. A.; Wöll, C. Controlling Interpenetration in Metal−Organic Frameworks by Liquid-phase Epitaxy. *Nat. Mater.* **2009**, *8*, 481−484.

(8) Zacher, D.; Shekhah, O.; Wöll, C.; Fischer, R. A. Thin Films of Metal−Organic Frameworks. *Chem. Soc. Rev.* **2009**, *38*, 1418−1429.

(9) Hermes, S.; Schröder, F.; Chelmowski, R.; Wöll, C.; Fischer, R. A. Selective Nucleation and Growth of Metal−Organic Open Framework Thin Films on Patterned $COOH/CF_3$-Terminated Self-Assembled Monolayers on Au(111). *J. Am. Chem. Soc.* **2005**, *127*, 13744−13745.

(10) Shekhah, O.; Liu, J.; Fischer, R. A.; Wöll, C. MOF Thin Films: Existing and Future Applications. *Chem. Soc. Rev.* **2011**, *40*, 1081−1106.

(11) Mondal, P. C.; Gera, B.; Gupta, T. *Advanced Organic-Inorganic Composites: Materials Device and Allied Applications;* Nova Science Publishers, Inc.: New York, 2012; Chapter 2, pp 1−33.

(12) Singh, V.; Mondal, P. C.; Lakshmanan, J. Y.; Zharnikov, M.; Gupta, T. Turn On Electron-Transfer-Based Selective Detection of Ascorbic Acid via Copper Complexes Immobilized on Glass. *Analyst* **2012**, *137*, 3216−3219.

(13) Tsekouras, G.; Johansson, O.; Lomoth, R. A Surface-Attached Ru Complex Operating as a Rapid Bistable Molecular Switch. *Chem. Commun.* **2009**, *23*, 3425−3427.

(14) Kumar, A.; Chhatwal, M.; Mondal, P. C.; Singh, V.; Singh, A. K.; Cristaldi, D. A.; Gupta, R. D.; Gulino, A. A Ternary Memory Module Using Low-Voltage Control over Optical Properties of Metal-Polypyridyl Monolayers. *Chem. Commun.* **2014**, *50*, 3783−3785.

(15) Facchetti, A.; Beverina, L.; van der Boom, M. E.; Dutta, P.; Evmenenko, G.; Shukla, A. D.; Stern, C. E.; Pagani, G. A.; Marks, T. J. Strategies for Electro-optic Film Fabrication. Influence of Pyrrole-Pyridine-Based Dibranched Chromophore Architecture on Covalent Self-Assembly, Thin-Film Microstructure, and Nonlinear Optical Response. *J. Am. Chem. Soc.* **2006**, *128*, 2142−2153.

(16) Terada, K.; Kanaizuka, K.; Iyer, V. M.; Sannodo, M.; Saito, S.; Kobayashi, K.; Haga, M. Memory Effects in Molecular Films of Free-Standing Rod-Shaped Ruthenium Complexes on an Electrode. *Angew. Chem., Int. Ed.* **2011**, *123*, 641−641.

(17) Fleming, C. N.; Maxwell, K. A.; DeSimone, J. M.; Meyer, T. J.; Papanikolas, J. M. Ultrafast Excited-State Energy Migration Dynamics in an Efficient Light-Harvesting Antenna Polymer Based on Ru(II) and Os(II) Polypyridyl Complexes. *J. Am. Chem. Soc.* **2001**, *123*, 10336−10347.

(18) Brown, D. G.; Sanguantrakun, N.; Schulze, B.; Schubert, U. S.; Berlinguette, C. P. Bis(tridentate) Ruthenium-Terpyridine Complexes Featuring Microsecond Excited-State Lifetimes. *J. Am. Chem. Soc.* **2012**, *134*, 12354−12357.

(19) Meyer, T. J. Chemical Approaches to Artificial Photosynthesis. *Acc. Chem. Res.* **1989**, *22*, 163−170.

(20) Sun, L. C.; Hammarström, L.; Åkermark, B.; Styring, S. Towards Artificial Photosynthesis: Ruthenium−Manganese Chemistry for Energy Production. *Chem. Soc. Rev.* **2001**, *30*, 36−49.

(21) Puntoriero, F.; Sartorel, A.; Orlandi, M.; La Ganga, G.; Serroni, S.; Bonchio, M.; Scandola, F.; Campagna, S. Photoinduced Water Oxidation using Dendrimeric Ru(II) Complexes as Photosensitizers. *Coord. Chem. Rev.* **2011**, *255*, 2594−2601.

(22) O'Regan, B.; Grätzel, M. A Low-Cost, High-Efficiency Solar Cell based on Dye-sensitized Colloidal TiO_2 Films. *Nature* **1991**, *353*, 737−740.

(23) Grätzel, M. Recent Advances in Sensitized Mesoscopic Solar Cells. *Acc. Chem. Res.* **2009**, *42*, 1788−1798.

(24) Singh, V.; Mondal, P. C.; Chhatwal, M.; Jeyachandran, Y. L.; Zharnikov, M. Catalytic Oxidation of Ascorbic Acid via Copper−Polypyridyl Complex Immobilized on Glass. *RSC Adv.* **2014**, *4*, 23168−23176.

(25) Singh, V.; Mondal, P. C.; Kumar, A.; Jeyachandran, Y. L.; Awasthi, S. K.; Gupta, R. D.; Zharnikov, M. Surface-Confined Heteroleptic Copper(II)−Polypyridyl Complexes for Photonuclease Activity. *Chem. Commun.* **2014**, *50*, 11484−11487.

(26) Gupta, T.; Mondal, P. C.; Kumar, A.; Jeyachandran, Y. L.; Zharnikov, M. Surface-Confined Heterometallic Molecular Dyads: Merging the Optical and Electronic Properties of Fe, Ru, and Os Terpyridyl Complexes. *Adv. Funct. Mater.* **2013**, *23*, 4227−4235.

(27) Mondal, P. C.; Lakshmanan, J. Y.; Hamoudi, H.; Zharnikov, M.; Gupta, T. Bottom-Up Assembly of Multicomponent Coordination-Based Oligomers. *J. Phys. Chem. C* **2011**, *115*, 16398−16404.

(28) Tuccitto, N.; Ferri, V.; Cavazzin, M.; Quici, S.; Zhavnerko, G.; Licciardello, A.; Rampi, M. A. Highly Conductive ∼ 40-nm-long Molecular Wires Assembled by Stepwise Incorporation of Metal Centres. *Nat. Mater.* **2009**, *8*, 41−46.

(29) Musumeci1, C.; Zappalà, G.; Martsinovich, N.; Orgiu, E.; Schuster, S.; Quici, S.; Zharnikov, M.; Troisi, A.; Licciardello, A.; Samorì, P. Nanoscale Electrical Investigation of Layer-by-Layer Grown Molecular Wires. *Adv. Mater.* **2014**, *26*, 1688−1693.

(30) Ishida, T.; Terad, K.; Hasegawa, K.; Kuwahata, H.; Kusama, K.; Sato, R.; Nakano, M.; Naitoh, Y.; Haga, M. Self-assembled Monolayer and Multilayer Formation using Redox-active Ru Complex with Phosphonic Acids on Silicon Oxide Surface. *Appl. Surf. Sci.* **2009**, *255*, 8824−8830.

(31) Altman, M.; Shukla, A. D.; Zubkov, T.; Evmenenko, G.; Dutta, P.; van der Boom, M. E. Controlling Structure from the Bottom-Up: Structural and Optical Properties of Layer-by-Layer Assembled Palladium Coordination-Based Multilayers. *J. Am. Chem. Soc.* **2006**, *128*, 7374−7382.

(32) Constable, E. C.; Thompson, A. M. W. C. Pendant-Functionalised Ligands for Metallo-supramolecular Assemblies; Ruthenium(II) and Osmium(II) Complexes of 4′-(4-Pyridy1)-2,2′:6′,2″-terpyridine. *J. Chem. Soc., Dalton Trans.* **1994**, *9*, 1409−1418.

(33) Constable, E. C. 2,2′:6′,2″-Terpyridines: From Chemical Obscurity to Common Supramolecular Motifs. *Chem. Soc. Rev.* **2007**, *36*, 246−253.

(34) de Ruiter, G.; Tartakovsky, E.; Oded, N.; van der Boom, M. E. Sequential Logic Operations with Surface-Confined Polypyridyl Complexes Displaying Molecular Random Access Memory Features. *Angew. Chem., Int. Ed.* **2010**, *49*, 169−172.

(35) Moulder, J. F.; Stickle, W. F.; Sobol, P. E.; Bomben, K. D. *Handbook of X-ray Photoelectron Spectroscopy;* Chastain, J., King, R. C., Jr., Eds.; Perkin-Elmer Corp.: Eden Prairie, MN, 1992.

(36) Stöhr, J. *NEXAFS Spectroscopy: Springer Series in Surface Science* 25; Springer-Verlag: Berlin, Germany, 1992.

(37) Hamoudi, H.; Döring, K.; Chesneau, F.; Lang, H.; Zharnikov, M. Self-Assembly of Pyridine-Substituted Alkanethiols on Gold: The Electronic Structure Puzzle in the Ortho- and Para-Attachment of Pyridine to the Molecular Chain. *J. Phys. Chem. C* **2012**, *116*, 861−870.

DOI: 10.1021/acsami.5b00953
ACS Appl. Mater. Interfaces 2015, 7, 8677−8686

(38) Darlatt, E.; Traulsen, C. H.-H.; Poppenberg, J.; Richter, S.; Kühn, J.; Schalley, C. A.; Unger, W. E. S. Evidence of Click and Coordination Reactions on a Self-Assembled Monolayer by Synchrotron Radiation based XPS and NEXAFS. *J. Electron Spectrosc. Relat. Phenom.* **2012**, *185*, 85−89.
(39) Darlatt, E.; Nefedov, A.; Traulsen, C. H.-H.; Poppenberg, J.; Richter, S.; Dietrich, P. M.; Lippitz, A.; Illgen, R.; Kühn, J.; Schalley, C. A.; Wöll, C.; Unger, W. E. S. Interpretation of Experimental N K NEXAFS of Azide, 1,2,3-Triazole and Terpyridyl Groups by DFT Spectrum Simulations. *J. Electron Spectrosc. Relat. Phenom.* **2012**, *185*, 621−624.
(40) Zharnikov, M.; Shaporenko, A.; Paul, A.; Gölzhäuser, A.; Scholl, A. X-ray absorption spectro-microscopy studies for the development of lithography with a monomolecular resist. *J. Phys. Chem. B* **2005**, *109*, 5168−5174.
(41) Kolczewski, C.; Puttner, R.; Plashkevych, O.; Agren, H.; Staemmler, V.; Martins, M.; Snell, G.; Schlachter, A. S.; Sant'Anna, M.; Kaindl, G.; Pettersson, L. G. M. Detailed Study of Pyridine at the C1s and N1s Ionization Thresholds: The Influence of the Vibrational Fine Structure. *J. Chem. Phys.* **2001**, *115*, 6426−6437.
(42) Mondal, P. C.; Chhatwal, M.; Jeyachandran, Y. L.; Zharnikov, M. Enhancement of Optical and Electrochemical Properties via Bottom-Up Assembly of Binary Oligomer System. *J. Phys. Chem. C* **2014**, *118*, 9578−9587.
(43) Mondal, P. C.; Singh, V.; Bhaskaran, S. Fe-Terpyridyl Complex Based Multiple Switches for Application in Molecular Logic Gates and Circuits. *New J. Chem.* **2014**, *38*, 2679−2685.
(44) Li, D.; Swanson, B. I.; Robinson, J. M.; Hoffbauer, M. A. Porphyrin based Self-Assembled Monolayer Thin Films: Synthesis and Characterization. *J. Am. Chem. Soc.* **1993**, *115*, 6975−6980.
(45) Bard, A. J.; Faulkner, L. R. *Electrochemical Methods: Fundamentals and Applications,* 2nd ed.; John Wiley & Sons: New York, 2001.
(46) Forster, R. J.; Faulkner, L. R. Interfacial Field Effects on Reductive Chloride Elimination from Spontaneously Adsorbed Monolayers. *Langmuir* **1995**, *11*, 1014−1023.
(47) Sharp, M.; Petersson, M.; Edstrom, K. Preliminary Determinations of Electron Transfer Kinetics Involving Ferrocene Covalently Attached to a Platinum Surface. *J. Electroanal. Chem.* **1979**, *95*, 123−130.
(48) Sierra, M.; Herranz, M. A.; Zhang, S.; Sanchez, L.; Martin, N.; Echegoyen, L. Self-Assembly of C_{60} π-Extended Tetrathiafulvalene (exTTF) Dyads on Gold Surfaces. *Langmuir* **2006**, *22*, 10619−10624.
(49) Boole, G. *An Investigation of the Laws of Thought;* Dover: New York, 1958.
(50) Ball, P. Chemistry Meets Computing. *Nature* **2000**, *406*, 118−120.
(51) de Silva, A. P. Molecular Computing: A Layer of Logic. *Nature* **2008**, *454*, 417−418.
(52) de Silva, A. P.; Uchiyama, S.; Vance, T. P.; Wannalerse, B. A Supramolecular Chemistry Basis for Molecular Logic and Computation. *Coord. Chem. Rev.* **2007**, *251*, 1623−1632.
(53) de Ruiter, G.; van der Boom, M. E. Surface-Confined Assemblies and Polymers for Molecular Logic. *Acc. Chem. Res.* **2011**, *44*, 563−573.
(54) Zhang, X.; Lee, S.; Liu, Y.; Lee, M.; Yin, J.; Sessler, J. S.; Yoon, J. Anion-activated, Thermoreversible Gelation System for the Capture, Release, and Visual Monitoring of CO_2. *Sci. Rep.* **2014**, *4*, 4593.
(55) Gupta, T.; Cohen, R.; Evmenenko, G.; Dutta, P.; van der Boom, M. E. Reversible Redox-Based Optical Sensing of Parts per Million Levels of Nitrosyl Cation in Organic Solvents by Osmium Chromophore-Based Monolayers. *J. Phys. Chem. C* **2007**, *111*, 4655−4660.
(56) Upadahyay, K. K.; Kumar, A.; Mishra, R. K.; Fyles, T. M.; Upadahyay, S.; Thapliyal, K. Reversible Colorimetric Switching of Thiophene Hydrazone based on Complementary IMP/INH Logic Functions. *New J. Chem.* **2010**, *34*, 1862−1866.

DOI: 10.1021/acsami.5b00953
ACS Appl. Mater. Interfaces 2015, 7, 8677−8686